Surface and Subsurface Hydrogen: Adsorption Properties on Transition Metals and Near-Surface Alloys

Jeff Greeley and Manos Mavrikakis*

Department of Chemical and Biological Engineering, University of Wisconsin—Madison, Madison, Wisconsin 53706

Received: August 2, 2004; In Final Form: November 20, 2004

Periodic, self-consistent DFT-GGA calculations are used to study the thermochemical properties of both surface and subsurface atomic hydrogen on a variety of pure metals and near-surface alloys (NSAs). For *surface hydrogen* on pure metals, calculated site preferences, adsorption geometries, vibrational frequencies, and binding energies are reported and are found to be in good agreement with available experimental data. On NSAs, defined as alloys wherein a solute is present near the surface of a host metal in a composition different from the bulk composition, surface hydrogen generally binds more weakly than it binds to the pure-metal components composing the alloys. Some of the NSAs even possess the unusual property of binding hydrogen as weakly as the noble metals while, at the same time, dissociating H_2 much more easily. On both NSAs and pure metals, formation of surface hydrogen is generally exothermic with respect to H_2(g). In contrast, formation of *subsurface hydrogen* is typically endothermic with respect to gas-phase H_2 (the only exception to this general statement is found for pure Pd). As with surface H, subsurface H typically binds more weakly to NSAs than to the corresponding pure-metal components of the alloys. The diffusion barrier for hydrogen from surface to subsurface sites, however, is usually lower on NSAs compared to the pure-metal components, suggesting that population of subsurface sites may occur more rapidly on NSAs.

Introduction

Hydrogenation, dehydrogenation, and hydrogenolysis processes are crucially important to the chemical industry, and a significant fraction of these processes are performed on heterogeneous transition-metal catalysts.[1−3] Although the chemistries that occur on these materials are often very complex, the behavior of hydrogen itself can have a substantial impact on the overall catalyst performance. Thus, to understand and improve upon currently existing transition-metal catalysts, it is useful to have a thorough understanding of the properties of hydrogen on a wide variety of catalytically relevant transition metals.

An enormous number of single-crystal studies have been undertaken to probe the behavior of atomic and molecular hydrogen on various transition-metal surfaces. A thorough review of this literature is beyond the scope of the present contribution (for a detailed summary of older hydrogen literature, the reader is referred to an excellent review by Christmann).[4] Thus, we simply present a broad outline of the research that has been performed in this area, focusing our attention primarily on the closest-packed surfaces of the pure metals and metal alloys that we have investigated in the present study.

Studies of hydrogen adsorption on pure metals are plentiful. The H/Ru(0001),[5−19] H/Pd(111),[20−40] H/Fe(110),[41−50] H/Pt(111),[51−61] H/Ni(111),[42,62−79] and H/W(110)[80−92] systems have been particularly well studied, and significant bodies of literature also exist for hydrogen on Cu(111),[93−97] Ag(111),[98−101] Mo(110),[82,83,91,102,103] Rh(111),[104−109] Re(0001),[21,110−112] and Ir(111).[113−115] Less information is available for hydrogen on Ta(110) and V(110).[116−118] From this work has emerged a picture of relatively facile H_2 dissociation on, and strong binding of atomic H to, most transition metals. The exceptions to this general conclusion are the noble metals (Cu, Ag, and Au), where binding is weaker and where H_2 dissociation is highly activated.

Publications focusing on the behavior of hydrogen on transition-metal alloys are somewhat less plentiful, but an important body of literature has nonetheless begun to accumulate. Of particular interest for the present work are studies of hydrogen behavior on near-surface alloys (NSAs). NSAs, defined as alloys wherein the composition near the surface differs from the bulk composition, may form even when bulk alloys are not thermodynamically stable,[119−121] and they can lead to dramatic changes in adsorbate reactivity compared to the corresponding pure-metal components. The unusual effects of NSAs on hydrogen chemisorption[122−127] and dissociation kinetics[128,129] have been demonstrated in a small, but growing, number of cases; recently, a computational analysis of both thermochemical and kinetic properties of hydrogen on a broad variety of idealized NSAs (where the surface layer is composed of either pure solute, an overlayer, or pure host, a subsurface alloy) has confirmed the generality of the unusual hydrogen−NSA interactions.[130]

Although the thermochemical and kinetic properties of hydrogen on metal *surfaces* are of primary interest for many technological and scientific applications, the characteristics of *subsurface* hydrogen are also important in some cases. Palladium and palladium-alloy membranes, for example, show great promise for hydrogen-separation and -purification processes.[131−133] Various metals and alloys (in the form of metal hydrides) may also be useful for hydrogen-storage applications.[134] Finally, the role of subsurface hydrogen in some catalytic processes, particularly hydrogenation reactions on nickel catalysts, may be significant.[135]

* To whom correspondence should be addressed. Phone: (608) 262-9053. Fax: (608) 262-5434. E-mail: manos@engr.wisc.edu.

10.1021/jp046540q CCC: $30.25 © 2005 American Chemical Society
Published on Web 01/25/2005

In this contribution, we use density functional theory (DFT) to analyze the thermochemical properties of both surface and subsurface hydrogen at a total coverage of $^1/_4$ ML (ML = monolayer) on a variety of pure transition metals and idealized NSAs (see the description above). We present an extensive database of binding energies (BEs), vibrational frequencies, magnetic properties, and structural data for surface hydrogen on various pure metals and alloys, and we attempt to correlate these properties with electronic structure characteristics of the respective clean metal surfaces. We then present similar results for subsurface hydrogen on a select group of pure metals and NSAs. Finally, we study the energetics of hydrogen diffusion from surface to subsurface sites, and we comment on the potential relevance of these subsurface species for various catalytic processes.

Methods

DACAPO, the total energy calculation code,[136] is used in this study. For all calculations, a four-layer slab, periodically repeated in a super-cell geometry with five equivalent layers of vacuum between any two successive metal slabs, is used. A 2×2 unit cell is employed, and the top two layers of the slab are allowed to relax. Adsorption is allowed on only one of the two exposed surfaces, and the electrostatic potential is adjusted accordingly.[137] Ionic cores are described by ultrasoft pseudopotentials,[138] and the Kohn−Sham one-electron valence states are expanded in a basis of plane waves with kinetic energy below 25 Ry. The surface Brillouin zone is sampled at 18 special Chadi−Cohen k points for (111) and (0001) surfaces and 16 special k points for (110) surfaces. In all cases, convergence of the total energy with respect to the k-point set and with respect to the number of metal layers included is confirmed. The exchange-correlation energy and potential are described self-consistently within the generalized gradient approximation (GGA-PW91);[139,140] non-self-consistent RPBE results[136] are also presented in some cases (reported energies are PW91 values unless RPBE is explicitly specified). The self-consistent PW91 density is determined by iterative diagonalization of the Kohn−Sham Hamiltonian, Fermi population of the Kohn−Sham states ($k_BT = 0.1$ eV), and Pulay mixing of the resulting electronic density.[141] All total energies have been extrapolated to $k_BT = 0$ eV. Spin polarization effects are tested for and included where appropriate. Zero-point-energy (ZPE) corrections are included in the reported results only where explicitly specified.

For the surface-to-subsurface diffusion-barrier calculations, we fix the z coordinate of the diffusing hydrogen atom at various positions along the diffusion coordinate. We allow all other degrees of freedom of the hydrogen and metal atoms to relax.

Vibrational frequencies are calculated by numerical differentiation of the forces using a second-order finite-difference approach with a step size of 0.015 Å. The metal atoms are fixed in their relaxed geometries for these calculations; only the hydrogen atom is displaced from its equilibrium position. This approximation is not expected to introduce significant error into the results because hydrogen and metal modes generally have frequencies differing by many hundreds of wavenumbers and are thus essentially decoupled. The Hessian matrix is mass-weighted and diagonalized to yield the frequencies and normal modes of the system.

The structures of the idealized NSAs considered in this study are described with the notation "X*/Y" or "X/Y". In both cases, X refers to the solute, and Y denotes the host. An asterisk (*) indicates that the solute is present in the form of an overlayer; the absence of an asterisk indicates that the system forms a subsurface alloy, with the solute in the layer right below the surface.

The calculated PW91 bond energy for H_2(g) is 4.57 eV. This result implies a ZPE-corrected value of ~4.30 eV, in fair agreement with the experimental value of 4.52 eV at 298 K.[142] Modification of calculated hydrogen-binding-energy (BE_H) values (with gas-phase H_2 as the reference state) to account for this modest theoretical/experimental discrepancy would result in a slight but systematic BE decrease (weaker binding) from the values reported below.

Results

In this section, we first present results for *surface* hydrogen. We analyze the chemical and physical properties of this species on a variety of pure metals and idealized NSAs (see the schematics in Figure 1). NSA structures in a vacuum are estimated with the segregation energy database of Ruban et al.,[143] and the particular NSAs studied are selected so as to be stable with respect to hydrogen-induced surface reconstructions.[130] Although the chosen NSA structures are clearly idealizations of real NSA surfaces, they should provide a good guide to realistic NSA chemistry.[130] We discuss the energetic, magnetic, and geometric features of the preferred binding configurations for hydrogen on the above pure metals and NSAs at $^1/_4$ ML coverage, we report vibrational frequencies and diffusion-barrier estimates for selected surfaces, and we discuss correlations in the hydrogen-binding trends across the transition metals. Second, we present BE results for *subsurface* hydrogen on pure metals and on Pt- and Pd-based NSAs. Finally, for a select group of pure metals and NSAs, we analyze thermochemical and kinetic barriers for surface−subsurface hydrogen diffusion (the thermochemical barrier is defined as the energy difference between surface and subsurface hydrogen, and the kinetic barrier denotes the activation energy for hydrogen diffusion between the surface and subsurface regions).

Surface Hydrogen. The BEs of the most favorable adsorption configurations for surface hydrogen, together with near-degenerate (though less favorable) configurations, are listed in Table 1; the magnetic moments per naturally magnetized metal atom are also given where appropriate, values for the metal work-function change upon hydrogen adsorption are indicated, and the distances (perpendicular to the surface plane) between adsorbed hydrogen and the nearest-neighbor surface metal atoms are tabulated. From Table 1, it is seen that, with relatively few exceptions, hydrogen prefers adsorption in hollow sites. For face-centered-cubic (fcc) and hexagonal-close-packed (hcp) metals [with (111) and (0001) surfaces, respectively], 3-fold fcc and hcp sites are preferred, and for body-centered-cubic (bcc) metals [with (110) surfaces], quasi-3-fold sites are favored. For Ir(111), however, the top site is favored by ~0.1 eV over the next most stable site, and for certain Pt-terminated NSAs [Ir/Pt(111), Re/Pt(111), W/Pt(111), Pt*/Ru(0001), and Pt*/Re(0001)], the top site is also weakly favored. Selected other Pt-terminated NSAs exhibit top-site adsorption that, while not actually energetically favored, is nonetheless close in energy to 3-fold-site adsorption. The metal work-function changes are generally modest for both the pure metals and the NSAs; values ranging from about −0.15 eV to about +0.45 eV are found. Ni(111), Co(0001), and Fe(110) slabs with adsorbed hydrogen have magnetic moments of 0.69, 1.66, and 2.53 μ_B per metal atom, respectively (these values represent decreases on the order of 0.02 μ_B/atom from the corresponding clean-slab magnetizations). Interestingly, when these elements are alloyed with platinum in an NSA configuration, the magnetizations (on a

TABLE 1: Binding energy (BE), Magnetic Moment (per Naturally Magnetized Metal Atom), Work-Function Change on Hydrogen Adsorption, and Perpendicular Distance of Hydrogen to the Plane of Nearest-Neighbor Surface Metal Atoms ($d_{H-metal}$) of *Surface* Hydrogen on the Close-Packed Surfaces of Various Transition Metals and Transition-Metal Alloys[a-c]

metal[d,e]	site[f]	BE (eV)	BE(RPBE) (eV)	magnetic moment (μ_B)	work-function change (eV)	$d_{H-metal}$ (Å)[g]	clean-surface ϵ_d (eV)
Ag	fcc	−2.08	−1.92		0.11	0.82	−4.10
	hcp	−2.06	−1.90		0.12	0.83	−4.10
Au	fcc	−2.22	−2.07		−0.16	0.65	−3.33
	hcp	−2.17	−2.02		−0.14	0.69	−3.33
Ir	top	−2.74	−2.62		−0.04	1.59	−2.85
Pt	fcc	−2.72	−2.55		−0.06	0.84	−2.52
	hcp	−2.68	−2.50		−0.06	0.85	−2.52
	top	−2.66	−2.53		−0.16	1.56	−2.52
Cu	fcc	−2.39	−2.23		0.08	0.89	−2.52
	hcp	−2.38	−2.21		0.09	0.90	−2.52
Re	fcc	−3.04	−2.90		−0.07	1.01	−2.07
	hcp	−3.01	−2.88		−0.13	1.06	−2.07
Rh	fcc	−2.81	−2.65		0.01	0.96	−2.02
	hcp	−2.80	−2.64		0.02	0.94	−2.02
Ru	fcc	−2.97	−2.81		0.03	1.05	−1.89
	hcp	−2.93	−2.77		0.05	1.04	−1.89
Pd	fcc	−2.88	−2.68		0.04	0.78	−1.81
	hcp	−2.84	−2.65		0.05	0.78	−1.81
Ni	fcc	−2.89	−2.71	0.69	0.02	0.90	−1.56
	hcp	−2.88	−2.70	0.69	0.03	0.90	−1.56
Co	fcc	−2.89	−2.69	1.66	−0.04	0.95	−1.48
	hcp	−2.86	−2.67	1.66	−0.04	0.94	−1.48
W	3-fold hollow	−3.15	−3.03		−0.02	1.07	−1.47
Mo	3-fold hollow	−3.05	−2.92		0.02	1.09	−0.99
Fe	3-fold hollow	−2.99	−2.78	2.53	−0.04	0.93/0.94	−0.90
	4-fold hollow	−2.93	−2.74	2.53	−0.04	0.94	−0.90
Ta	3-fold hollow	−3.24	−3.14		−0.14	1.04/1.10	−0.30
V	3-fold hollow	−3.29	−3.15		−0.11	1.04/1.07	0.03
W/Pt	top	−2.30	−2.17		0.37	1.63	−3.29
Ta/Pt	fcc	−2.15	−1.99		0.20	0.88	−3.29
	hcp	−2.15	−1.99		0.22	0.87	−3.29
V/Pt	fcc	−2.15	−2.00		0.13	0.92	−3.24
	hcp	−2.17	−2.02		0.13	0.87	−3.24
	top	−2.12	−2.00		0.44	1.64	−3.24
Re/Pt	top	−2.45	−2.32		0.33	1.62	−3.20
Mo/Pt	hcp	−2.26	−2.10		0.14	0.86	−3.10
	fcc	−2.26	−2.09		0.06	0.90	−3.10
	top	−2.25	−2.13		0.39	1.62	−3.10
Fe/Pt	hcp	−2.35	−2.18	3.88	0.00	0.84	−2.88
	fcc	−2.35	−2.17	3.87	−0.01	0.84	−2.88
Ir/Pt	top	−2.58	−2.45		−0.02	1.59	−2.87
	fcc	−2.57	−2.40		−0.01	0.93	−2.87
	hcp	−2.53	−2.36		−0.01	0.91	−2.87
Ru/Pt	fcc	−2.53	−2.36		0.03	0.91	−2.82
	hcp	−2.52	−2.34		0.02	0.88	−2.82
	top	−2.49	−2.35		0.06	1.59	−2.82
Co/Pt	hcp	−2.44	−2.26	2.86	−0.01	0.83	−2.78
	fcc	−2.43	−2.24	2.85	0.00	0.84	−2.78
Rh/Pt	fcc	−2.57	−2.41		−0.03	0.88	−2.70
	hcp	−2.55	−2.38		−0.03	0.86	−2.70
Ni/Pt	fcc	−2.54	−2.35	1.61	−0.05	0.82	−2.60
	hcp	−2.53	−2.37	1.62	−0.05	0.82	−2.60
Cu/Pt	fcc	−2.68	−2.49		−0.18	0.80	−2.37
	hcp	−2.67	−2.48		−0.18	0.81	−2.37
Ta/Pd	fcc	−2.27	−2.12		0.28	0.85	−2.78
	hcp	−2.28	−2.12		0.23	0.78	−2.78
V/Pd	fcc	−2.30	−2.15		0.22	0.86	−2.74
	hcp	−2.34	−2.18		0.16	0.77	−2.74
W/Pd	fcc	−2.37	−2.20		0.31	0.90	−2.73
	hcp	−2.36	−2.19		0.30	0.87	−2.73
Re/Pd	fcc	−2.50	−2.33		0.35	0.90	−2.64
	hcp	−2.45	−2.27		0.36	0.87	−2.64
Mo/Pd	fcc	−2.44	−2.26		0.23	0.83	−2.55
	hcp	−2.43	−2.25		0.23	0.80	−2.55
Fe/Pd	fcc	−2.46	−2.29	3.75	0.13	0.79	−2.44
	hcp	−2.48	−2.30	3.76	0.12	0.79	−2.44
Ir/Pd	fcc	−2.71	−2.53		0.19	0.90	−2.32
	hcp	−2.66	−2.48		0.19	0.88	−2.32
Ru/Pd	fcc	−2.64	−2.47		0.24	0.86	−2.31
	hcp	−2.61	−2.43		0.26	0.85	−2.31

TABLE 1 (Continued)

metal[d,e]	site[f]	BE (eV)	BE(RPBE) (eV)	magnetic moment (μ_B)	work-function change (eV)	$d_{H-metal}$ (Å)[g]	clean-surface ϵ_d (eV)
Re/Rh	fcc	−2.64	−2.47		0.15	0.97	−2.28
	hcp	−2.61	−2.44		0.17	0.94	−2.28
Ir/Rh	fcc	−2.76	−2.59		0.03	0.98	−2.17
	hcp	−2.75	−2.58		0.04	0.96	−2.17
Mo/Rh	fcc	−2.66	−2.49		0.06	0.93	−2.16
V/Rh	fcc	−2.58	−2.42		0.07	0.95	−2.13
	hcp	−2.55	−2.41		0.02	0.88	−2.13
Ru/Rh	fcc	−2.83	−2.66		0.06	0.97	−2.05
	hcp	−2.83	−2.66		0.06	0.97	−2.05
Pt*/Ru	top	−2.42	−2.28		−0.15	1.58	−2.98
	fcc	−2.42	−2.25		−0.09	0.98	−2.98
	hcp	−2.42	−2.25		−0.08	0.97	−2.98
Pd*/Ru	fcc	−2.61	−2.42		0.12	0.91	−2.36
	hcp	−2.61	−2.42		0.12	0.90	−2.36
Rh*/Ru	fcc	−2.86	−2.69		0.07	0.96	−2.02
	hcp	−2.84	−2.67		0.08	0.94	−2.02
Pt*/Re	top	−2.56	−2.43		0.08	1.61	−3.37
Pd*/Re	fcc	−2.55	−2.37		0.40	1.01	−2.73
	hcp	−2.53	−2.36		0.40	1.00	−2.73
Rh*/Re	fcc	−2.68	−2.52		0.32	1.07	−2.50

[a] All near-surface alloys are stable with respect to hydrogen-induced compositional changes near the surface. [b] The reference state is gas-phase atomic hydrogen and the clean metal slab at infinite separation from one another. [c] BEs of −2.28 (PW91) and −2.29 (RPBE) eV correspond to thermoneutral dissociative adsorption of H_2(g). [d] Asterisks (*) denote ideal overlayer near-surface alloys; other near-surface alloys are ideal subsurface alloys (see schematics in Figure 1). [e] The pure metals and each family of near-surface alloys are listed in order of increasing ϵ_d of the corresponding clean surface. [f] Sites (fcc, hcp, or top) with BEs within 0.06 eV of the best site are shown. [g] Multiple entries for a given distance indicate that the perpendicular distance from hydrogen to the appropriate nearest-neighbor metal atoms is not uniform for all of the metal atoms.

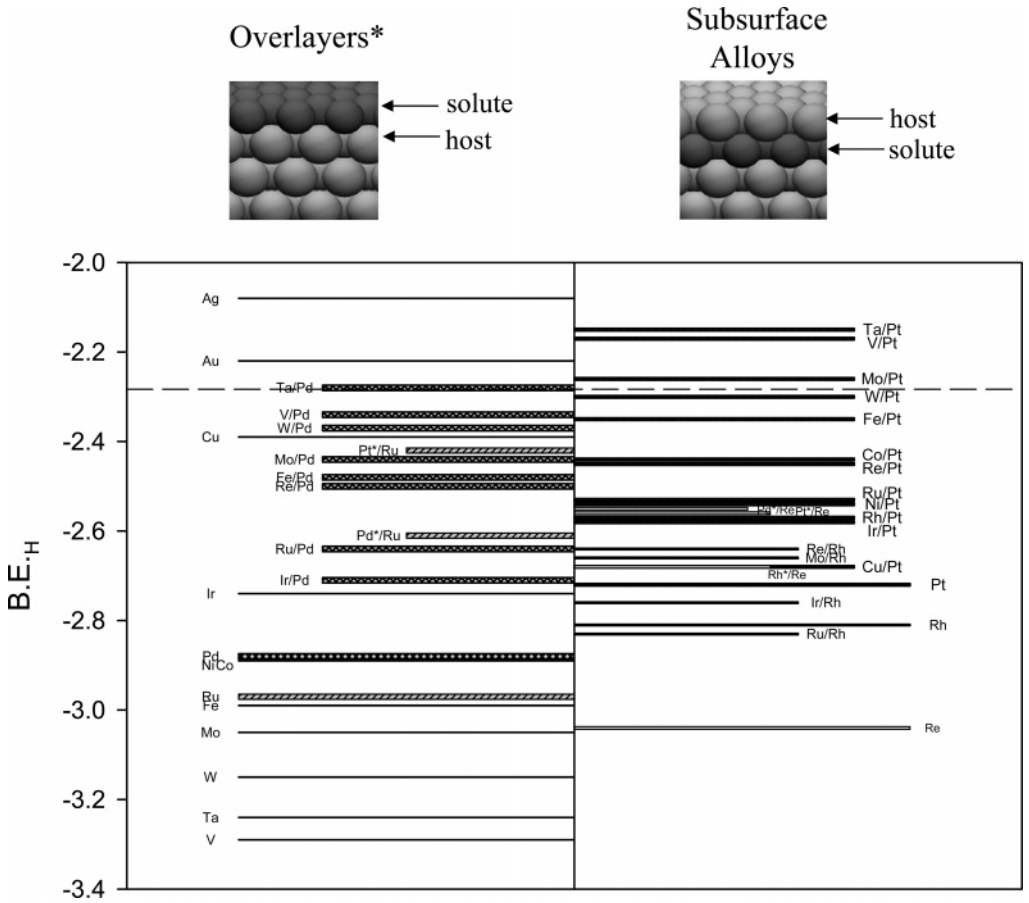

Figure 1. Hydrogen binding energies values on various close-packed surfaces, referenced to a clean metal slab and a gas-phase atomic hydrogen, H(g), at infinite separation from one another. Asterisks (*) denote overlayer NSAs; all other NSAs are subsurface alloys (see also schematics). Both the length and the sign of the bars associated with the various alloys and pure metals are arbitrary and are varied only for clarity. The horizontal dashed line denotes thermoneutral dissociative adsorption of H_2.

per Ni, Co, or Fe basis) respectively increase to 1.61, 2.86, and 3.88 μ_B (with reductions of ∼0.05 μ_B from the respective clean slabs), suggesting that a nonmagnetic metal, platinum, tends to enhance the natural magnetic characteristics of Ni, Co, and Fe. A similar result is found for naturally magnetic solutes alloyed with Pd; for Fe/Pd(111), for example, the magnetic moment

TABLE 2: Estimated Surface Diffusion Barriers for Surface Hydrogen on the Closest-Packed Surfaces of Selected Transition Metals and Near-Surface Alloys

metal	surface diffusion barrier[a]	diffusion pathway[b]
Ag	0.13	fcc−bridge−hcp
Au	0.12	fcc−bridge−hcp
Ir	0.13	top−fcc−top
Pt	0.04	fcc−bridge−hcp
Cu	0.15	fcc−bridge−hcp
Re	0.17	fcc−bridge−hcp
Rh	0.11	fcc−bridge−hcp
Ru	0.14	fcc−bridge−hcp
Pd	0.15	fcc−bridge−hcp
Ni	0.14	fcc−bridge−hcp
Co	0.16	fcc−bridge−hcp
W	0.08	qt−sb−qt
	0.24	qt−lb−qt
Mo	0.14	qt−sb−qt
	0.18	qt−lb−qt
Fe	0.15	qt−sb−qt
	0.06	qt−lb−qt
Ta	0.26	qt−sb−qt
	0.15	qt−lb−qt
V	0.31	qt−sb−qt
	0.08	qt−lb−qt
W/Pt	0.09	top−fcc−top
Re/Pt	0.08	top−fcc−top
Ru/Pt	0.03	fcc−bridge−hcp
Ni/Pt	0.07	fcc−bridge−hcp

[a] All energies are reported in eV. [b] qt = quasi-3-fold. sb = short bridge. lb = long bridge.

per Fe atom is 3.76 μ_B [a 0.05 μ_B reduction from the Fe/Pd(111) clean slab]. None of the other pure elements or alloys examined in this study are found to have a nonzero magnetic moment. Finally, Table 1 indicates that the perpendicular hydrogen−metal distance in 3-fold sites varies between ∼0.7 and ∼1.1 Å across the fcc/hcp metals and their alloys. When hydrogen is adsorbed on top sites, the perpendicular hydrogen−metal distance is ∼1.6 Å for all of the metals and alloys considered here.

Atomic hydrogen surface diffusion-barrier estimates, and the corresponding diffusion paths, for selected pure metals and NSAs are presented in Table 2. The barriers, which are estimated from the difference in BEs at the sites indicated in the table, are generally small; values of 0.10−0.15 eV are typical for both pure metals and alloys. Thus, it is expected that hydrogen will diffuse rapidly on most of these surfaces.

BE_H data for the most favorable adsorption configurations are presented in the form of a spectrum in Figure 1. The figure indicates that a modest range of BE_H values exists, ranging from endothermic [compared to $H_2(g)$] adsorption on pure Ag and Au (BE_H values of −2.08 and −2.22 eV, respectively) to very strong binding on W, Ta, and V (BE_H values of −3.15, −3.24, and −3.29 eV, respectively). The BE_H values on NSAs fall primarily between these two extremes, forming a quasi-continuous spectrum of BEs between the reactive base metals and the unreactive coinage metals.

Subsurface Hydrogen. The BEs and preferred sites for subsurface hydrogen are listed in Table 3; the magnetic moments per naturally magnetized metal atom are also given where appropriate, and the distances (perpendicular to the surface plane) between absorbed hydrogen and the nearest-neighbor metal atoms in both the surface and subsurface metal layers are tabulated. Two subsurface sites, the octahedral (under fcc) and the tetrahedral II (under top) sites, are favorably occupied by hydrogen [the tetrahedral I (under hcp) site is only favorably occupied on Pt and Pd]. For the majority of the metals and alloys considered, a clear preference for one or the other of these sites is found (this is in contrast to the situation with surface hydrogen, where the fcc and hcp sites generally have comparable BEs). In a few cases (Pt, Pd, Fe/Pt, Co/Pt, Rh/Pt, Ni/Pt, and V/Pd), however, two or more quasi-degenerate subsurface configurations do exist. The range of subsurface BEs is ∼1.5 eV (see Figure 2); this is slightly larger than the corresponding range of surface BEs (∼1.25 eV). The strongest subsurface binding is found for Pd (BE = −2.53 eV), while the weakest is found for Ir (BE = −1.06 eV). Interestingly, Pd is the only metal considered with an exothermic formation energy for subsurface hydrogen, although Cu/Pt(111) (−2.22 eV), V/Pd-(111) (−2.20 eV), and Ni(111) (−2.19 eV) have only weakly endothermic formation energies.

The magnetic moments (per naturally magnetized metal atom) for pure Ni, Co, and Fe with subsurface hydrogen (0.68, 1.67, and 2.53 μ_B, respectively; Table 3) are similar to the corresponding moments with surface hydrogen. Alloying these metals with platinum increases the magnetic moments (on a per Ni, Co, or Fe basis) to ∼1.46, 2.75, and 3.84 μ_B, respectively, again

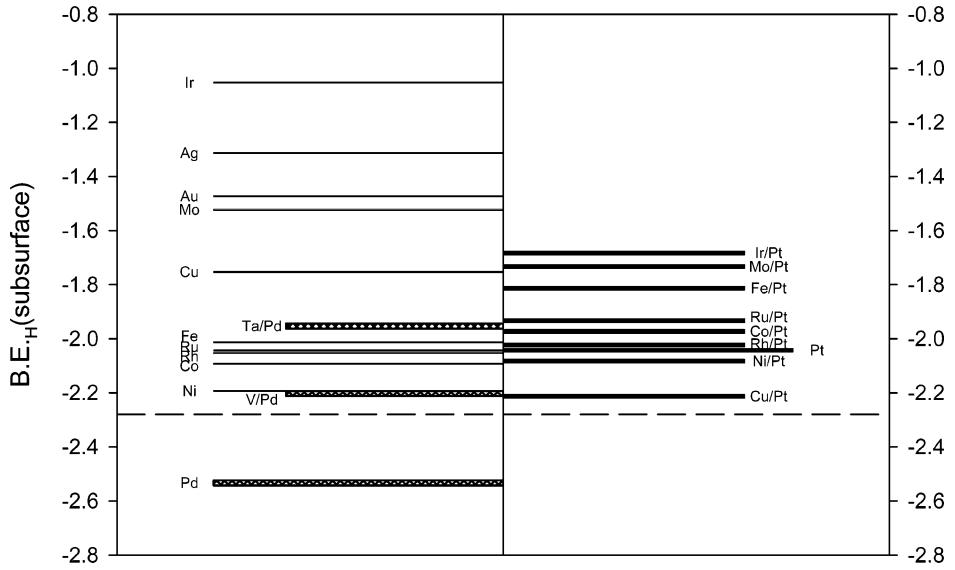

Figure 2. Subsurface hydrogen binding energies on various close-packed surfaces, referenced to a clean metal slab and a gas-phase atomic hydrogen, H(g), at infinite separation from one another. See also Figure 1 caption.

TABLE 3: Binding Energy (BE) of *Subsurface* Hydrogen on the Close-Packed Surfaces of Various Pure Metals and Near-Surface Alloys[a−d]

metal	preferred site[e]	BE (eV)	BE(RPBE) (eV)	magnetic moment (μ_B)[f]	$d_{H-surface}$ (Å)[g]	$d_{H-subsurface}$ (Å)[h]
Ag	tetra II	−1.31	−1.18		1.95	0.68
Au	tetra II	−1.47	−1.36		1.90	0.81
Ir	tetra II	−1.06	−0.92		1.62	0.97
Pt	tetra I	−2.04	−1.89		0.60	1.90
	tetra II	−2.04	−1.90		1.69	1.00
Cu	octahedral	−1.75	−1.58		0.55	1.64
Rh	octahedral	−2.05	−1.89		0.83	1.41
Ru	octahedral	−2.04	−1.89		0.83/0.86[i]	1.33
Pd	octahedral	−2.53	−2.35		0.78	1.58
	tetra I	−2.53	−2.33		0.58	1.84
	tetra II	−2.49	−2.32		1.72	0.84
Ni	octahedral	−2.19	−1.99	0.68	0.94	1.13
Co	octahedral	−2.09	−1.88	1.67	0.94	1.07
Mo	underbridge	−1.53	−1.38		1.09	1.24
Fe	underbridge	−2.01	−1.81	2.53	1.06	1.08
Mo/Pt	octahedral	−1.73	−1.59		0.87	1.45
Fe/Pt	octahedral	−1.82	−1.63	3.84	0.54	1.57
	tetra II	−1.77	−1.58	3.69	1.78	0.40
Ir/Pt	tetra II	−1.68	−1.54		1.76	0.81
Ru/Pt	octahedral	−1.93	−1.77		0.80	1.49
Co/Pt	tetra II	−1.97	−1.77	2.75	1.75	0.36
	octahedral	−1.97	−1.79	2.83	0.71	1.37
Rh/Pt	tetra II	−2.02	−1.87		1.74	0.73
	octahedral	−1.98	−1.82		0.73	1.56
Ni/Pt	tetra II	−2.08	−1.90	1.46	1.76	0.37
	octahedral	−2.03	−1.88	1.56	0.69	1.41
Cu/Pt	octahedral	−2.22	−2.03		0.50	1.63
Ta/Pd	octahedral	−1.96	−1.81		0.98	1.35
V/Pd	octahedral	−2.20	−2.07		1.06	1.11
	tetra II	−2.16	−2.02		1.87	0.30

[a] The indicated near-surface alloys are ideal subsurface alloys. [b] All near-surface alloys are stable with respect to hydrogen-induced changes in composition near the surface. [c] The reference state is gas-phase atomic hydrogen and the clean metal slab at infinite separation from one another. [d] BEs of −2.28 (PW91) and −2.29 (RPBE) eV correspond to thermoneutral dissociative absorption of H_2(g). [e] Sites (octahedral, below surface fcc sites; tetrahedral I, below surface hcp sites; tetrahedral II, directly below surface metal atoms) with BEs within 0.06 eV of the best site are shown. [f] The magnetic moment is given per naturally magnetized metal atom in the presence of absorbed hydrogen. [g] $d_{H-surface}$ = perpendicular distance of hydrogen to the plane of nearest-neighbor surface metal atoms. [h] $d_{H-subsurface}$ = perpendicular distance of hydrogen to the plane of nearest-neighbor subsurface (second layer) metal atoms. [i] Multiple entries for a given distance indicate that the perpendicular distance from hydrogen to the appropriate nearest-neighbor metal atoms is not uniform for all of the metal atoms.

comparable to the corresponding results with surface hydrogen. Finally, the sixth column of Table 3 gives the perpendicular distances between subsurface hydrogen and the nearest-neighbor surface metal atoms, and the seventh column indicates the perpendicular distances between hydrogen and the nearest-neighbor subsurface metal atoms. Hydrogen in octahedral sites is substantially closer to the surface metal layer than to the subsurface layer; this observation holds for both pure metals and for NSAs. In the tetrahedral II (under top) sites, however, the reverse is true; hydrogen is closer to the subsurface layer. Again, this result seems to hold both for pure metals and for alloys.

The energetic results for selected pure metals and NSAs (Tables 1 and 3) are summarized in Figure 3. The horizontal dashed line is the zero of the energy scale, corresponding to H_2(g) and the clean metal slabs at infinite separation from one another. The metals and alloys are shown in order of increasing surface d-band center (ϵ_d; Table 1). Figure 4 is a plot of the thermochemical barriers for surface-to-subsurface diffusion (the difference in energies between the best surface and best subsurface sites) on all Pt- and Pd-based NSAs for which the thermochemistry of both surface and subsurface hydrogen has been analyzed (Tables 1 and 3); the kinetic diffusion barriers, where available, are superimposed on these values. With the exception of the Ir/Pt(111) subsurface alloy, the thermochemical diffusion barriers on the NSAs are seen to be lower than the barriers for the corresponding pure host.

Table 4 lists the calculated harmonic vibrational frequencies, together with available experimental values, for surface hydrogen in the most favorable binding sites on selected pure metals and NSAs; the corresponding ZPEs are also tabulated. For both pure metals and alloys, surface hydrogen has two degenerate or near-degenerate vibrational modes and one mode of higher frequency. The mode of higher frequency is typically ∼1050 cm^{-1} for 3-fold sites and ∼2050 cm^{-1} for top sites; the degenerate modes vary in frequency from 300−500 cm^{-1} (top sites) to 500−1000 cm^{-1} (3-fold sites). The magnitude of the total ZPE (including all three vibrational modes) for a given hydrogen atom is significant (∼0.15 eV in most cases). However, the ZPE correction to the products of dissociative H_2 adsorption (two H atoms) is approximately equal to the ZPE of gas-phase H_2; thus, the net ZPE correction for dissociative H_2 adsorption is generally small.

Figure 5 is a plot of the non-ZPE-corrected BEs of both surface and subsurface hydrogen against the ϵ_d values of the corresponding clean metal surfaces (Tables 1 and 3). For the Pt-based subsurface alloys, it is seen that there are separate linear correlations for surface and subsurface hydrogen. Similar correlations exist for the pure metals, although the scatter in the data is somewhat greater than is the scatter for the Pt-based alloys.

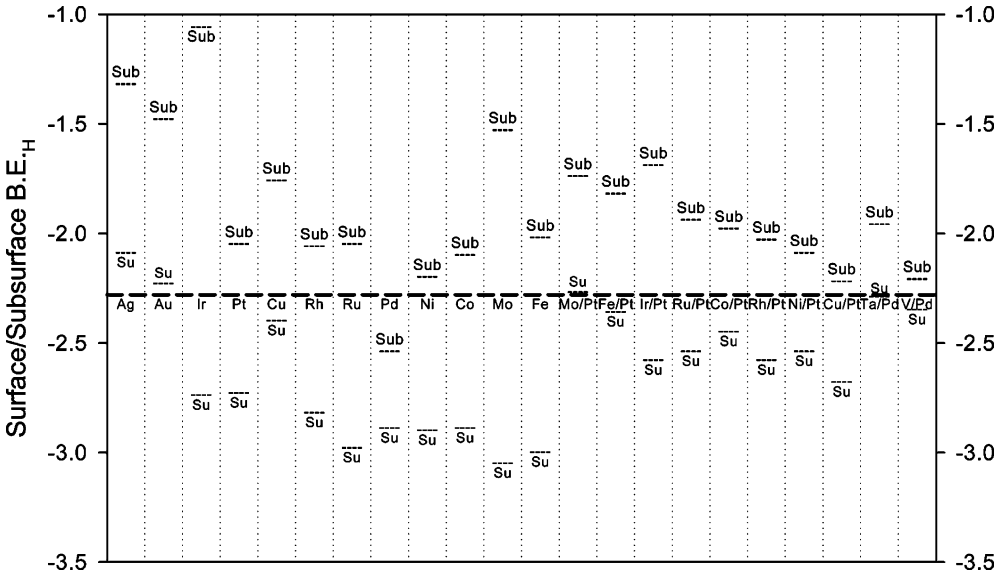

Figure 3. BEs of surface and subsurface hydrogen, referenced to a clean metal slab and a gas-phase hydrogen atom, H(g), at infinite separation from one another. Sub = subsurface. Su = surface. The horizontal dashed line denotes thermoneutral dissociative adsorption/absorption of H_2.

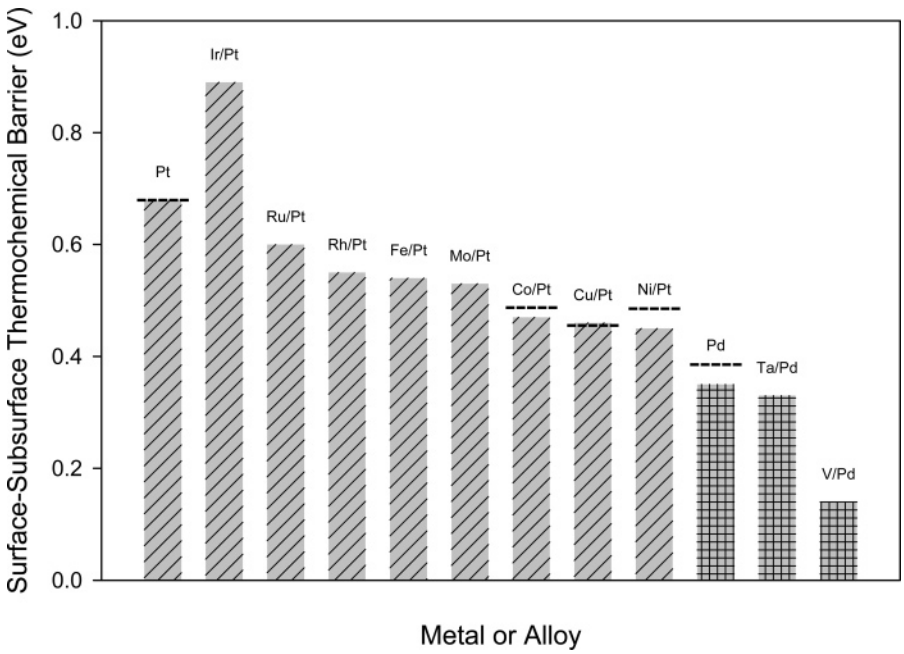

Figure 4. Thermochemical and kinetic barriers for diffusion of hydrogen from surface to subsurface. Bars with diagonal lines are Pt or Pt-based ideal subsurface alloys, and bars with crosshatches represent Pd or Pd-based ideal subsurface alloys. The bar height gives the thermochemical diffusion barrier. Horizontal dashed lines denote the kinetic barrier for hydrogen surface-to-subsurface diffusion processes.

Discussion

Hydrogen on Pure-Metal Surfaces. The thermochemical binding characteristics of surface atomic hydrogen presented above are largely consistent with available experimental and theoretical data. First, the general, calculated preference of surface hydrogen for 3-fold sites (Table 1) is in excellent agreement with a variety of experimental and computational studies on pure-metal single crystals.[9,19,31,33,53,63,64,82,95,99,144,145] Good agreement is also found for the unusual case of Ir(111), where hydrogen prefers top-site adsorption (see work by Hagedorn et al.[113] and Krekelberg et al.[145] for detailed discussions of this case). Far fewer studies exist with which to compare our calculated site preferences for surface hydrogen on NSAs, but the good agreement found on pure metals suggests that the NSA site preferences are likely to be accurate (similar arguments apply to the calculated site preferences for subsurface hydrogen on pure- and alloy-metal surfaces). Second, geometric parameters calculated for hydrogen adsorption on pure metals agree well with experimental results. For example, on Ni(111), experimental measurements suggest a hydrogen-surface distance of 0.98 ± 0.08 Å,[42] in agreement with our calculated value of 0.92 Å (note that the H position is compared to the clean-metal-surface position for this value, in contrast to the convention adopted in Table 1). On Mo(110), a H−Mo bond length of 1.93 Å is estimated from LEED measurements;[146] the corresponding calculated value in the present study (not reported in Table 1) is 1.95−2.06 Å (we find that the distances of the H atom in the quasi-3-fold site to the three adjacent Mo atoms are not equivalent). On W(110), VLEED was used to measure a H−W bond length of 2.09 Å;[92] our calculated range of 1.92−2.05 Å [see comments for Mo(110)] is in reasonable agreement with this value. On Fe(110), a LEED-determined H−Fe distance of

TABLE 4: Calculated Harmonic Vibrational Frequencies and Zero-Point Energies (ZPEs) of *Surface* Hydrogen on Various Transition Metals and Transition-Metal Near-Surface Alloys[a−e]

metal	site	calcd frequencies (cm^{-1})	experimental frequencies (cm^{-1})	calcd ZPE (eV)
Ag	fcc	766, 770, 793	703, 857[f]	0.14
Au	fcc	738, 746, 815		0.14
Ir	top	456(2), 2168	540, 2030[g]	0.19
Pt	fcc	589, 592, 1043	250, 548[h]	0.14
	top	344, 352, 2213		0.18
Cu	fcc	873, 878, 1015	807, 1043[i]	0.17
Rh	fcc	743, 753, 1085	639−728, 1116[j]	0.16
Ru	fcc	792, 812, 1115	695, 1075[k]	0.17
Pd	fcc	871, 876, 954	776, 1003[l]	0.17
Ni	fcc	891, 909, 1154	765, 1100[m]	0.18
Co	fcc	879, 885, 1139		0.18
W	3-fold hollow	762, 826, 1250	550, 770, 1250[n]	0.18
Mo	3-fold hollow	781, 817, 1163	710, 1071[o]	0.17
Fe	3-fold hollow	768, 919, 1074	880, 1060[p]	0.17
Mo/Pt	fcc	676, 682, 948		0.14
	top	440(2), 2010		0.18
Fe/Pt	fcc	742, 750, 973		0.15
Ir/Pt	top	388(2), 2115		0.18
	fcc	554, 562, 1023		0.13
Ru/Pt	fcc	625, 626, 982		0.14
	top	340, 351, 2094		0.17
Co/Pt	hcp	711, 716, 1019		0.15
Rh/Pt	fcc	639, 646, 1006		0.14
	top	323, 326, 2134		0.17
Ni/Pt	fcc	724, 730, 983		0.15
Cu/Pt	fcc	749, 754, 1012		0.16
Ru/Pd	fcc	823, 829, 949		0.16

[a] Experimental frequencies are listed where available. [b] All near-surface alloys shown here are ideal subsurface alloys and are stable with respect to hydrogen-induced changes in composition near the surface. [c] The ZPEs refer to a single hydrogen atom. [d] The ZPE of H_2(g) is 0.27 eV. [e] To illustrate the effect of site preference on ZPE, ZPEs for both 3-fold and top sites are reported for selected pure metals and alloys. [f] Lee, G.; Plummer, E. W. *Phys. Rev. B: Condens. Matter Mater. Phys.* **1995**, *51*, 7250. [g] Hagedorn, C. J.; Weiss, M. J.; Weinberg, W. H. *Phys. Rev. B: Condens. Matter Mater. Phys.* **1999**, *60*, R14 016. [h] Badescu, S. C.; Salo, P.; Ala-Nissila, T.; Ying, S. C.; Jacobi, K.; Wang, Y.; Bedürftig, K.; Ertl, G. *Phys. Rev. Lett.* **2002**, *88*, 1361011-1−1361011-4. [i] Lee, G.; Plummer, E. W. *Surf. Sci.* **2002**, *498*, 229. [j] Yanagita, H.; Fujioka, H.; Aruga, T.; Takagi, N.; Nishijima, M. *Surf. Sci.* **1999**, *441*, 507. [k] Conrad, H.; Scala, R.; Stenzel, W.; Unwin, R. *J. Chem. Phys.* **1984**, *81*, 6371. [l] Conrad, H.; Kordesch, M. E.; Scala, R.; Stenzel, W. *J. Electron Spectrosc. Relat. Phenom.* **1986**, *38*, 289. [m] Johnson, A. D.; Maynard, K. J.; Daley, S. P.; Yang, Q. Y.; Ceyer, S. T. *Phys. Rev. Lett.* **1991**, *67*, 927. [n] Balden, M.; Lehwald, S.; Ibach, H. *Phys. Rev. B: Condens. Matter Mater. Phys.* **1996**, *53*, 7479. [o] Kroger, J.; Lehwald, S.; Ibach, H. *Phys. Rev. B: Condens. Matter Mater. Phys.* **1997**, *55*, 10 895. [p] Baró, A. M.; Erley, W. *Surf. Sci.* **1981**, *112*, L759.

1.75 Å[44] agrees well with our calculated value of 1.78 Å, and on Pd(111), a LEED value of 1.78 ± 0.05 Å[31] for the H−Pd distance is close to our value of 1.82 Å.

Third, although we sometimes overestimate available experimental results, our calculated BE_H values are in reasonable agreement with these values (Table 5). We note, in passing, that inherent limitations in the accuracy of temperature-programmed desorption (TPD) techniques, together with differences in coverage between the experiments and our calculations, may explain some of the reported experimental/theoretical differences. TPD spectra of H_2 desorption from Ru(0001) give an estimated energy change of 1.28 eV;[147] this agrees well with our calculated PW91 value of 1.37 eV for H_2 desorption. TPD has also been used to determine adsorption energies for hydrogen on Ni(111);[62,63] the value of about −0.50 eV (gas-phase H_2 reference) obtained in those experiments is slightly less than our calculated value of −0.61 eV (−2.89 eV with respect to gas-phase atomic H). On Ir(111), an H_2 desorption barrier of 0.55 eV has been measured with thermal desorption mass spectronomy (TDMS).[114] This barrier is somewhat less than the 0.91 eV barrier implied by Table 5; the addition of ZPE corrections to the theoretical value (Table 4), however, gives a desorption energy of 0.80 eV, in better agreement with the experimental results. On Pt(111), a D_2 desorption barrier of 0.69 ± 0.07 eV was determined with TPD; our calculated energy change for D_2 desorption, 0.88 eV, appears to slightly overestimate this value (ZPE corrections do not change the calculated result in this particular case). On Pd(111),

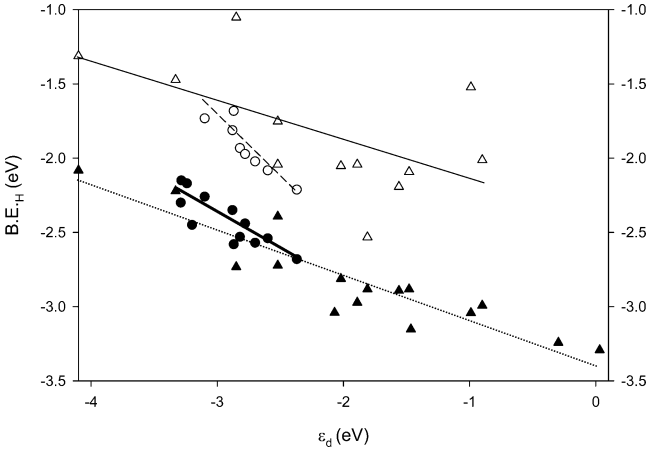

Figure 5. Binding energy (BE) versus surface *d*-band center (ϵ_d) correlations for surface and subsurface hydrogen. Solid circles and thick solid line = surface H on Pt ideal subsurface alloys. Open circles and long-dashed line = subsurface H on Pt ideal subsurface alloys. Solid triangles and thin dotted line = surface H on pure metals. Open triangles and thin solid line = subsurface H on pure metals.

TABLE 5: Calculated and Measured Desorption Energies (DE) for Surface Hydrogen on the Close-Packed Surfaces of Selected Transition Metals[a−d]

metal	PW91 DE	RPBE DE	experimental DE
Ir	0.91	0.65	0.55[e]
Pt	0.88	0.53	0.69 ± 0.07[f]
Rh	1.06	0.72	0.81[g]
Ru	1.37	1.04	1.28[h]
Pd	1.19	0.79	0.90[i]
Ni	1.22	0.85	1.00[j], 0.98[k]
Co	1.21	0.81	0.69[l]
W	1.74	1.48	1.52[m]
Mo	1.53	1.26	1.47[n]
Fe	1.42	0.98	1.13[o]

[a] Calculated results are given for both the PW91 and RPBE functionals. [b] DE is defined as the energy change for the removal of two H atoms from the surface to form gas-phase H_2; DE = −2BE − 4.57, where 4.57 is the PW91 bond energy of gas-phase H_2 (4.58 for RPBE). [c] BE is defined as the binding energy of atomic hydrogen, referenced to gas-phase atomic H and a clean metal slab at infinite separation from one another. [d] All energies are reported in eV. [e] Engstrom, J. R.; Tsai, W.; Weinberg, W. H. *J. Chem. Phys.* 1987, *87*, 3104. [f] Norton, P. R.; Davies, J. A.; Jackman, T. E. *Surf. Sci.* 1982, *121*, 103. [g] Yates, J. T.; Thiel, P. A.; Weinberg, W. H. *Surf. Sci.* 1979, 427. [h] Jachimowski, T. A.; Meng, B.; Johnson, D. F.; Weinberg, W. H. *J. Vac. Sci. Technol. A* 1995, *13*, 1564. [i] Conrad, H.; Ertl, G.; Latta, E. E. *Surf. Sci.* 1974, *41*, 435. [j] Christmann, K.; Schober, O.; Ertl, G.; Neumann, M. *J. Chem. Phys.* 1974, *60*, 4528. [k] Lapujoulade, J.; Neil, K. S. *J. Chem. Phys.* 1972, *57*, 3535. [l] Bridge, M. E.; Comrie, C. M.; Lambert, R. M. *J. Catal.* 1979, *58*, 28. [m] Nahm, T. U.; Gomer, R. *Surf. Sci.* 1997, *375*, 281−292. [n] Mahnig, M.; Schmidt, L. D. *Z. Phys. Chem.* 1972, *80*, 71. [o] Bozso, F.; Ertl, G.; Grunze, M.; Weiss, M. *Appl. Surf. Sci.* 1977, *1*, 103.

an H_2 desorption heat of ~0.90 eV was measured with TDS;[148] our values of 1.19 eV (1.12 eV with ZPE effects included) modestly overestimate the experimental results. On W(110), low-coverage H_2 desorption energies of 1.52 eV (isosteric desorption techniques[84]) and 1.41 eV (TPD[149]) have been measured; the calculated value of 1.74 eV (1.65 eV with ZPE corrections) is, again, somewhat larger than the experimental results. On Rh(111), TDMS measurements gave an H_2 desorption energy of ~0.81 eV,[150] slightly lower than our calculated value of 1.06 eV (1.01 eV with ZPE corrections). On Mo(110), flash desorption mass spectroscopy was used to find a high-binding-energy state with a desorption energy of 1.47 eV;[151] this value is in reasonable agreement with our calculated value of 1.53 eV (1.46 eV with ZPE corrections). On Fe(110), a desorption energy of 1.13 eV was found with TDS;[152] this result is somewhat lower than our calculated value of 1.42 eV (1.35 eV with ZPE corrections). On Co(0001), TDS measurements give a desorption energy of ~0.69 eV,[153] substantially less than our ZPE-corrected result of 1.12 eV.

The above results suggest that the PW91-GGA DFT calculations generally overestimate the magnitude of experimentally measured hydrogen-binding and -desorption energies. Interestingly, however, RPBE values are generally lower than the experimental results by a comparable amount (Table 5); the combination of the PW91 and RPBE results thus bounds the experimental values.[145] We note that, although ZPEs do not have a large effect on the calculated BEs, they generally lead to a lowering of the calculated BEs, thus bringing the PW91 values into better agreement with experiments. Finally, because the deviations of the calculated values from the experimental results are roughly constant for most of the pure transition metals analyzed in this study, we suggest that trends predicted using the theoretical results will reliably anticipate experimental trends.

A final comparison between our pure-metal results and experimental measurements involves the vibrational frequencies of adsorbed hydrogen. Our calculated frequencies generally reproduce experimental results reasonably well (Table 4). The highest frequency modes agree with those of the experiments to within ~50 cm^{-1}, or ~5% [the exceptions to this general trend of good agreement are found on Ir(111), where the favored site is, atypically, a top site, and on Pt(111), where anharmonic effects, not accounted for in the present calculations, are known to play a particularly significant role[53]]. The lower frequency modes are more difficult to determine theoretically; there, the calculations typically overestimate the experimental results by 100−150 cm^{-1}.

The above analyses demonstrate that our calculated site preferences, adsorption geometries, BEs, and vibrational frequencies on pure metals compare favorably to experimental values for these quantities. Where deviations between experimental and theoretical values do exist, the discrepancies generally involve roughly constant offsets from the experimental results, thus permitting the correct determination of trends across different metals from the theoretical results. Further, although very few experimental data exist with which to compare our calculated results on NSAs, we expect that the ability of our DFT calculations to accurately reproduce experimental trends will hold for these systems as well.

Hydrogen on NSAs. The BE spectrum for hydrogen on both NSAs and pure metals (Figure 1) clearly demonstrates that the noble metals (Au, Ag, and Cu) bind hydrogen very weakly ($BE_H \leq -2.39$ eV) while other transition metals exhibit considerably stronger binding (BE_H values of between −2.72 and −3.29 eV). The class of NSAs analyzed in this study generally exhibits weaker binding of hydrogen than do the pure, non-noble metals, in good agreement with the results of recent TPD experiments (we note, however, that most NSAs still bind hydrogen more strongly than do the pure, noble metals).[129,154]

Some of the NSAs considered in this study actually bind hydrogen as weakly as do the noble metals. These NSAs also show H−H scission transition states of considerably lower energy than those of the noble metals.[130] Thus, while Cu, Ag, and Au are inactive for processes involving the dissociation of H_2,[155,156] the NSAs have lower H−H scission barriers and may well be active for such processes. The NSAs, therefore, show a highly desirable combination of catalytic characteristics for hydrogenation reactions; the low BE_H values would allow them to be operated at low temperatures (thus increasing selectivity), and the low dissociation barriers would permit them to remain active for hydrogenation processes.

The BEs of surface and subsurface hydrogen across the various NSAs and pure metals can be qualitatively understood in terms of the electronic structure of the clean-surface metal atoms. The data in Figure 5 show that a reasonable linear correlation exists between the ϵ_d of Pt-terminated NSAs and the BE of both surface and subsurface hydrogen. The slopes of the $BE_H^{surface}$ and $BE_H^{subsurface}$ versus ϵ_d lines are approximately equal, but the intercept of the $BE_H^{subsurface}$ correlation is at a somewhat higher energy. The differing intercepts reflect the generally more endothermic binding of hydrogen to subsurface (as opposed to surface) sites; we note that a single correlation between surface and subsurface BE_H values and ϵ_d is not expected because of the greatly different interactions of the respective hydrogen states with their metal surroundings. Figure 5 also indicates that surface and subsurface BE_H values on pure transition metals correlate reasonably well with ϵ_d. There is more scatter in the pure-metal correlations, however, than there is in the correlations for Pt-terminated NSAs. The increased level of scatter may be the result of two effects; first, the overlap integrals of the respective pure-metal surfaces differ,[157] and second, the pure-metal correlations include data from metals with bcc crystal structures. The geometries of the surface and subsurface sites of bcc metals are different from the corresponding geometries of fcc and hcp metals, and such differences may lead to increased scatter in correlations that include a combination of metals of bcc and fcc (or hcp) crystal structures [we note that two of the data points that deviate the most from the best-fit line for subsurface hydrogen on pure metals (the ϵ_d values are about −1 eV for both data points) correspond to Fe(110) and Mo(110) surfaces].

Subsurface Hydrogen. The subsurface hydrogen data presented for pure metals and for selected NSAs (Table 3; Figures 2 and 3) demonstrate that, with the exception of pure Pd(111), the population of subsurface sites is energetically unfavorable with respect to H_2(g), at least at a coverage of $^1/_4$ ML. This result is consistent with a great body of literature that has shown the ability of Pd and Pd alloys to form subsurface/bulk hydrogen (see, e.g., refs 4 and 133) and with recent studies showing the difficulty of producing subsurface hydrogen on Ni(111) crystals.[66,158,159] Figure 2 also demonstrates that, generally speaking, subsurface hydrogen binds more weakly to Pt-based NSAs than it binds to pure Pt; the same result is observed for several Pd-based NSAs. This trend is similar to the result, described above, that NSAs generally bind surface hydrogen more weakly than do the pure (non-noble) transition metals. Notable exceptions to the trend of weakened subsurface hydrogen binding on NSAs are seen for Ni/Pt and for Cu/Pt. In those cases, subsurface hydrogen is more stable than it is on pure Pt; this result might

be partially explained by the significant expansive strain induced in the Ni and Cu subsurface layers as they accommodate the larger Pt lattice constant (such strain effects are not significant for surface hydrogen on these subsurface alloys; there, the H is screened from the strained subsurface layers by an intervening, unstrained Pt surface layer).

Although the observed weaker binding of subsurface hydrogen on NSAs might suggest that NSAs would not function well in hydrogen-storage applications, these alloys could, nonetheless, find uses in this area because of the decreased diffusion barriers that they exhibit for surface−subsurface penetration of H atoms. Figure 4 demonstrates that, for all Pt-based subsurface alloys except Ir/Pt, the energy change for diffusion of hydrogen from the surface to the subsurface is less endothermic than it is on pure Pt. The Pd-based NSAs analyzed in the present work show similar trends. We note that the kinetic diffusion barriers are nearly equal to the thermochemical barriers in all cases for which detailed kinetic calculations have been performed. Thus, while the weaker BE_H values suggest that very high hydrogen pressures might be needed to stabilize subsurface hydrogen on NSAs, the reduced diffusion barriers indicate that the kinetics of hydrogen penetration to subsurface sites might be considerably improved on these alloys.

Conclusions

The binding of atomic hydrogen to surface and subsurface sites on the close-packed surfaces of a large ensemble of pure metals and NSAs has been analyzed using periodic, self-consistent DFT-GGA calculations. Adsorption geometries, BEs, and vibrational frequencies for surface hydrogen show reasonable agreement with available experimental data. On NSAs, hydrogen is generally observed to bind more weakly than it binds to the corresponding pure metals, although the binding is still stronger than it is with most noble metals (the gap in BE_H values between the noble metals and the other pure transition metals is thus bridged by the NSAs). On some of the NSAs, a favorable combination of weak H binding and facile H_2 dissociation is observed, suggesting that these alloys might serve as improved hydrogenation catalysts. In general, subsurface hydrogen also binds more weakly to NSAs than to the corresponding pure host metal; population of subsurface sites is an endothermic process on all such alloys, as it is on all pure metals with the exception of Pd. Although the thermodynamics of subsurface H formation may be less favorable on NSAs than on pure transition metals, the diffusion barriers for H penetration into the subsurface are reduced on these alloys, suggesting that the kinetics of subsurface H formation may be improved on NSAs.

Acknowledgment. NSF supported this work through a CAREER Award (Grant CTS-0134561) to M.M. Additional partial support was provided by a DOE-BES Catalysis Science grant (Grant DE-FG02-03ER15469). Calculations were performed with National Energy Research Scientific Computing Center (NERSC) and Molecular Science Computing Facility (MSCF-PNNL) resources. We thank J. Chen for fruitful discussions.

References and Notes

(1) Satterfield, C. N. *Heterogeneous Catalysis in Industrial Practice*, 2nd ed.; Krieger Pulishing Company: Malabar, FL, 1996.
(2) Chorkendorff, I.; Niemantsverdriet, H. *Concepts of Modern Catalysis and Kinetics*; Wiley-VCH: Weinheim, Germany, 2003.
(3) Somorjai, G. A. *Introduction to Surface Chemistry and Catalysis*; John Wiley: New York, 1994.
(4) Christmann, K. *Surf. Sci. Rep.* **1988**, *9*, 1.
(5) Baddorf, A. P.; Jahns, V.; Zehner, D. M.; Zajonz, H.; Gibbs, D. *Surf. Sci.* **2002**, *498*, 74.
(6) Hammer, B. *Phys. Rev. B: Condens. Matter Mater. Phys.* **2001**, *63*, 205423.
(7) Jachimowski, T. A.; Weinberg, W. H. *J. Chem. Phys.* **1994**, *101*, 10997.
(8) Chou, M. Y.; Chelikowsky, J. R. *Phys. Rev. Lett.* **1987**, *59*, 1737.
(9) Schulz, J.; Taglauer, E.; Feulner, P.; Menzel, D. *Nucl. Instrum. Methods Phys. Res., Sect. B* **1992**, *64*, 588.
(10) Conrad, H.; Scala, R.; Stenzel, W.; Unwin, R. *J. Chem. Phys.* **1984**, *81*, 6371.
(11) Chou, M. Y.; Chelikowsky, J. R. *Phys. Rev. B: Condens. Matter Mater. Phys.* **1989**, *39*, 5623.
(12) Arena, M. V.; Westre, E. D.; Brown, D. E.; Kutzner, J.; George, S. M. *Surf. Sci.* **1995**, *325*, 151.
(13) Sun, Y. K.; Weinberg, W. H. *Surf. Sci.* **1989**, *214*, L246.
(14) Sokolowski, M.; Koch, T.; Pfnur, H. *Surf. Sci.* **1991**, *243*, 261.
(15) Shi, H.; Jacobi, K. *Surf. Sci.* **1994**, *313*, 289.
(16) Barteau, M. A.; Broughton, J. Q.; Menzel, D. *Surf. Sci.* **1983**, *133*, 443.
(17) Yates, J. T., Jr. *Surf. Sci.* **1985**, *160*, 37.
(18) Peden, C. H. F.; Goodman, D. W.; Houston, J. E.; Yates, J. T., Jr. *Surf. Sci.* **1988**, *194*, 92.
(19) Lindroos, M.; Pfnur, H.; Menzel, D. *Surf. Sci.* **1987**, *192*, 421.
(20) Nobuhara, K.; Nakanishi, H.; Kasai, H.; Okiji, A. *J. Appl. Phys.* **2000**, *88*, 6897.
(21) Pallassana, V.; Neurock, M.; Hansen, L. B.; Nørskov, J. K. *Phys. Rev. B: Condens. Matter Mater. Phys.* **1999**, *60*, 6146.
(22) Løvvik, O. M.; Olsen, R. A. *Phys. Rev. B: Condens. Matter Mater. Phys.* **1998**, *58*, 10890.
(23) Olsen, R. A.; Philipsen, P. H. T.; Baerends, E. J.; Kroes, G. J.; Løvvik, O. M. *J. Chem. Phys.* **1997**, *106*, 9286.
(24) Lober, R.; Hennig, D. *Phys. Rev. B: Condens. Matter Mater. Phys.* **1997**, *55*, 4761.
(25) Dong, W.; Kresse, G.; Furthmüller, J.; Hafner, J. *Phys. Rev. B: Condens. Matter Mater. Phys.* **1996**, *55*, 10952.
(26) Paul, J. F.; Sautet, P. *Surf. Sci.* **1996**, *356*, L403.
(27) Paul, J. F.; Sautet, P. *Phys. Rev. B: Condens. Matter Mater. Phys.* **1996**, *53*, 8015.
(28) Ezzehar, H.; Stauffer, L.; Dreysse, H.; Habar, M. *Surf. Sci.* **1995**, *333*, 144.
(29) Hsu, C. H.; Elbatanouny, M.; Martini, K. M. *J. Electron Spectrosc. Relat. Phenom.* **1990**, *54*, 353.
(30) Hsu, C. H.; Larson, B. E.; Elbatanouny, M.; Willis, C. R.; Martini, K. M. *Phys. Rev. Lett.* **1991**, *66*, 3164.
(31) Felter, T. E.; Sowa, E. C.; van Hove, M. A. *Phys. Rev. B: Condens. Matter Mater. Phys.* **1989**, *40*, 891.
(32) Stulen, R. H.; Kubiak, G. D. *J. Vac. Sci. Technol., A* **1987**, *5*, 535.
(33) Eberhardt, W.; Louie, S. G.; Plummer, E. W. *Phys. Rev. B: Condens. Matter Mater. Phys.* **1983**, *28*, 465.
(34) Conrad, H.; Kordesch, M. E.; Scala, R.; Stenzel, W. *J. Electron Spectrosc. Relat. Phenom.* **1986**, *38*, 289.
(35) Gdowski, G. E.; Felter, T. E. *J. Vac. Sci. Technol., A* **1986**, *4*, 1409.
(36) Felter, T. E.; Stulen, R. H. *J. Vac. Sci. Technol., A* **1985**, *3*, 1566.
(37) Felter, T. E.; Foiles, S. M.; Daw, M. S.; Stulen, R. H. *Surf. Sci.* **1986**, *171*, L379.
(38) Rick, S. W.; Doll, J. D. *Surf. Sci.* **1994**, *302*, L305.
(39) Gdowski, G. E.; Stulen, R. H.; Felter, T. E. *J. Vac. Sci. Technol., A* **1987**, *5*, 1103.
(40) Greuter, F.; Strathy, I.; Plummer, E. W.; Eberhardt, W. *Phys. Rev. B: Condens. Matter Mater. Phys.* **1986**, *33*, 736.
(41) Itsumi, Y.; Ellis, D. E. *J. Mater. Res.* **1996**, *11*, 2206.
(42) Hammer, L.; Landskron, H.; Nichtl-Pecher, H.; Fricke, A.; Heinz, K.; Müller, K. *Phys. Rev. B: Condens. Matter Mater. Phys.* **1993**, *47*, 15969.
(43) Minot, C.; Demangeat, C. *J. Chem. Phys.* **1987**, *86*, 2161.
(44) Moritz, W.; Imbihl, R.; Behm, R. J.; Ertl, G.; Matsushima, T. *J. Chem. Phys.* **1985**, *83*, 1959.
(45) Chemaschi, P.; Yang, H.; Whitten, J. L. *Surf. Sci.* **1995**, *330*, 255.
(46) Kurz, E. A.; Hudson, J. B. *Surf. Sci.* **1988**, *195*, 15.
(47) Kurz, E. A.; Hudson, J. B. *Surf. Sci.* **1988**, *195*, 31.
(48) Erley, W.; Baro, A. M. *Surf. Sci.* **1981**, *112*, L759.
(49) Imbihl, R.; Behm, R. J.; Christmann, K.; Ertl, G.; Matsushima, T. *Surf. Sci.* **1982**, *117*, 257.
(50) Nichtlpecher, W.; Gossmann, J.; Hammer, L.; Heinz, K.; Müller, K. *J. Vac. Sci. Technol., A* **1992**, *10*, 501.
(51) Nobuhara, K.; Kasai, H.; Nakanishi, H.; Okiji, A. *Surf. Sci.* **2002**, *507*, 82.
(52) Nobuhara, K.; Nakanishi, H.; Kasai, H.; Okiji, A. *J. Appl. Phys.* **2002**, *91*, 1855.
(53) Badescu, S. C.; Salo, P.; Ala-Nissila, T.; Ying, S. C.; Jacobi, K.; Wang, Y.; Bedürftig, K.; Ertl, G. *Phys. Rev. Lett.* **2002**, *88*, 136101-1−136101-4.

(54) Olsen, R. A.; Kroes, G. J.; Baerends, E. J. *J. Chem. Phys.* **1999**, *111*, 11155.
(55) Umezawa, K.; Ito, T.; Asada, M.; Nakanishi, S.; Ding, P.; Lanford, W. A.; Hjörvarsson, B. *Surf. Sci.* **1997**, *387*, 320.
(56) Wei, D.; Smith, K. E.; Kevan, S. D. *Phys. Rev. B: Condens. Matter Mater. Phys.* **1992**, *45*, 3652.
(57) Richter, L. J.; Ho, W. *Phys. Rev. B: Condens. Matter Mater. Phys.* **1987**, *36*, 9797.
(58) Seebauer, E. G.; Schmidt, L. D. *Chem. Phys. Lett.* **1986**, *123*, 129.
(59) Batra, I. P. *Surf. Sci.* **1984**, *137*, L97.
(60) Feibelman, P. J.; Hamann, D. R. *Surf. Sci.* **1987**, *182*, 411.
(61) Poelsema, B.; Palmer, R. L.; Mechtersheimer, G.; Comsa, G. *Surf. Sci.* **1982**, *117*, 60.
(62) Lapujoulade, J.; Neil, K. S. *J. Chem. Phys.* **1972**, *57*, 3535.
(63) Christmann, K.; Schober, O.; Ertl, G.; Neumann, M. *J. Chem. Phys.* **1974**, *60*, 4528.
(64) Christmann, K.; Behm, R. J.; Ertl, G.; Van Hove, M. A.; Weinberg, W. H. *J. Chem. Phys.* **1979**, *70*, 4168.
(65) Russell, J. N., Jr.; Chorkendorff, I.; Lanzillotto, A. M.; Alvey, M. D.; Yates, J. T., Jr. *J. Chem. Phys.* **1986**, *85*, 6186.
(66) Johnson, A. D.; Maynard, K. J.; Daley, S. P.; Yang, Q. Y.; Ceyer, S. T. *Phys. Rev. Lett.* **1991**, *67*, 927.
(67) Hanbicki, A. T.; Darling, S. B.; Gaspar, D. J.; Sibener, S. J. *J. Chem. Phys.* **1999**, *111*, 9053.
(68) van de Walle, G. F. A.; van Kempen, H.; Wyder, P.; Flipse, C. J. *Surf. Sci.* **1987**, *181*, 27.
(69) Winkler, A.; Rendulic, K. D. *Surf. Sci.* **1982**, *118*, 19.
(70) Cao, G. X.; Nabighian, E.; Zhu, X. D. *Phys. Rev. Lett.* **1997**, *79*, 3696.
(71) Okuyama, H.; Ueda, T.; Aruga, T.; Nishijima, M. *Phys. Rev. B: Condens. Matter Mater. Phys.* **2001**, *63*, 233403-1−233403-4.
(72) Premm, H.; Pölzl, H.; Winkler, A. *Surf. Sci.* **1998**, *401*, L444.
(73) Wright, S.; Skelly, J. F.; Hodgson, A. *Faraday Discuss.* **2000**, *117*, 133.
(74) Yang, H.; Whitten, J. L. *J. Chem. Phys.* **1993**, *98*, 5039.
(75) Kresse, G.; Hafner, J. *Surf. Sci.* **2000**, *459*, 287.
(76) Kaji, H.; Kakitani, K.; Yagi, Y.; Yoshimori, A. *Shinku* **2002**, *45*, 258.
(77) Zheng, H.; Rao, B. K.; Khanna, S. N.; Jena, P. *Phys. Rev. B: Condens. Matter Mater. Phys.* **1997**, *55*, 4174.
(78) Castellani, N. J.; Légaré, P.; Demangeat, C.; Pick, S. *Surf. Sci.* **1996**, *352*−*354*, 148.
(79) Sha, X.; Jackson, B. *Chem. Phys. Lett.* **2002**, *357*, 389.
(80) Chuikov, B. A.; Osovskii, V. D.; Ptushinskii, Y. G.; Sukretnyi, V. G. *Surf. Sci.* **2001**, *473*, 143.
(81) Osovskii, V. D.; Ptushinskii, Y. G.; Sukretnyi, V. G.; Chuikov, B. A. *JETP Lett.* **1998**, *67*, 959.
(82) Arnold, M.; Sologub, S.; Hupfauer, G.; Bayer, P.; Frie, W.; Hammer, L.; Heinz, K. *Surf. Rev. Lett.* **1997**, *4*, 1291.
(83) Kohler, B.; Ruggerone, P.; Scheffler, M. *Phys. Rev. B: Condens. Matter Mater. Phys.* **1997**, *56*, 13 503.
(84) Nahm, T. U.; Gomer, R. *Surf. Sci.* **1997**, *375*, 281.
(85) Altshuler, E. S.; Mills, D. L. *Surf. Sci.* **1996**, *367*, L91.
(86) Kwak, K. W.; Chou, M. Y.; Troullier, N. *Phys. Rev. B: Condens. Matter Mater. Phys.* **1996**, *53*, 13 734.
(87) Balden, M.; Lehwald, S.; Ibach, H. *Phys. Rev. B: Condens. Matter Mater. Phys.* **1996**, *53*, 7479.
(88) Hulpke, E.; Ludecke, J. *Phys. Rev. Lett.* **1992**, *68*, 2846.
(89) Raeker, T. J.; Depristo, A. E. *Surf. Sci.* **1990**, *235*, 84.
(90) Gaylord, R. H.; Kevan, S. D. *Phys. Rev. B: Condens. Matter Mater. Phys.* **1988**, *37*, 8491.
(91) Altman, M.; Chung, J. W.; Estrup, P. J.; Kosterlitz, J. M.; Prybyla, J.; Sahu, D.; Ying, S. C. *J. Vac. Sci. Technol., A* **1987**, *5*, 1045.
(92) Herlt, H. J.; Bauer, E. *Surf. Sci.* **1986**, *175*, 336.
(93) Lee, G.; Plummer, E. W. *Surf. Sci.* **2002**, *498*, 229.
(94) Kammler, T.; Küppers, J. *J. Chem. Phys.* **1999**, *111*, 8115.
(95) Gundersen, K.; Hammer, B.; Jacobsen, K. W.; Nørskov, J. K.; Lin, J. S.; Milman, V. *Surf. Sci.* **1993**, *285*, 27.
(96) McCash, E. M.; Parker, S. F.; Pritchard, J.; Chesters, M. A. *Surf. Sci.* **1989**, *215*, 363.
(97) Greuter, F.; Strathy, I.; Plummer, E. W.; Eberhardt, W. *Phys. Rev. B: Condens. Matter Mater. Phys.* **1986**, *33*, 736.
(98) Lee, G.; Plummer, E. W. *Phys. Rev. B: Condens. Matter Mater. Phys.* **2000**, *62*, 1651.
(99) Lee, G.; Plummer, E. W. *Phys. Rev. B: Condens. Matter Mater. Phys.* **1995**, *51*, 7250.
(100) Yu, C. F.; Hogg, C. S.; Sibener, S. J. *J. Electron Spectrosc. Relat. Phenom.* **1983**, *30*, 99.
(101) Zhou, X. L.; White, J. M.; Koel, B. E. *Surf. Sci.* **1989**, *218*, 201.
(102) Kroger, J.; Greber, T.; Osterwalder, J. *Phys. Rev. B: Condens. Matter Mater. Phys.* **2000**, *61*, 14 146.
(103) Kroger, J.; Lehwald, S.; Ibach, H. *Phys. Rev. B: Condens. Matter Mater. Phys.* **1997**, *55*, 10895.
(104) Yanagita, H.; Fujioka, H.; Aruga, T.; Takagi, N.; Nishijima, M. *Surf. Sci.* **1999**, *441*, 507.
(105) Seebauer, E. G.; Kong, A. C. F.; Schmidt, L. D. *J. Chem. Phys.* **1988**, *88*, 6597.
(106) Mate, C. M.; Somorjai, G. A. *Phys. Rev. B: Condens. Matter Mater. Phys.* **1986**, *34*, 7417.
(107) Mann, S. S.; Seto, T.; Barnes, C. J.; King, D. A. *Surf. Sci.* **1991**, *261*, 155.
(108) Santoro, G.; Franchini, A.; Bortolani, V. *Nuovo Cimento Soc. Ital. Fis., D* **1998**, *20*, 1055.
(109) Colonell, J. I.; Curtiss, T. J.; Sibener, S. J. *Surf. Sci.* **1996**, *366*, 19.
(110) Pallassana, V.; Neurock, M.; Hansen, L. B.; Nørskov, J. K. *J. Chem. Phys.* **2000**, *112*, 5435.
(111) Rodriguez, J. A.; Campbell, R. A.; Goodman, D. W. *Surf. Sci.* **1991**, *244*, 211.
(112) He, J. W.; Goodman, D. W. *J. Phys. Chem.* **1990**, *94*, 1502.
(113) Hagedorn, C. J.; Weiss, M. J.; Weinberg, W. H. *Phys. Rev. B: Condens. Matter Mater. Phys.* **1999**, *60*, R14016.
(114) Engstrom, J. R.; Tsai, W.; Weinberg, W. H. *J. Chem. Phys.* **1987**, *87*, 3104.
(115) Chakarov, D. V.; Marinova, T. S. *Surf. Sci.* **1998**, *204*, 147.
(116) Murgai, V.; Weng, S. L.; Strongin, M.; Ruckman, M. W. *Phys. Rev. B: Condens. Matter Mater. Phys.* **1983**, *28*, 6116.
(117) Kneedler, E.; Smith, K. E.; Skelton, D.; Kevan, S. D. *Phys. Rev. B: Condens. Matter Mater. Phys.* **1991**, *44*, 8233.
(118) Belov, V. D.; Ustinov, Y. K.; Komar, A. P. *Zh. Tekh. Fiz.* **1976**, *46*, 2403.
(119) Sinfelt, J. H. *Bimetallic Catalysts: Discoveries, Concepts, and Applications*; John Wiley and Sons: New York, 1983.
(120) Besenbacher, F.; Chorkendorff, I.; Clausen, B. S.; Hammer, B.; Molenbroek, A. M.; Nørskov, J. K.; Stensgaard, I. *Science* **1998**, *279*, 1913.
(121) Nielsen, L. P.; Besenbacher, F.; Stensgaard, I.; Laegsgaard, E.; Engdahl, C.; Stoltze, P.; Jacobsen, K. W.; Nørskov, J. K. *Phys. Rev. Lett.* **1993**, *71*, 754.
(122) Atli, A.; Abon, M.; Bertolini, J. C.; Boudeville, Y.; Fallavier, M.; Benmansour, M.; Thomas, J. P. *J. Phys. Chem.* **1994**, *98*, 4895.
(123) Hwu, H. H.; Eng, J., Jr.; Chen, J. G. *J. Am. Chem. Soc.* **2002**, *124*, 702.
(124) Kitchin, J. R.; Khan, N. A.; Barteau, M. A.; Chen, J. G.; Yakshinksiy, B.; Madey, T. E. *Surf. Sci.* **2003**, *544*, 295.
(125) Boo, J. B.; Lee, S. B.; Linke, R.; Becker, C.; Schroder, U.; Wandelt, K. *J. Korean Phys. Soc.* **1999**, *35*, S582.
(126) Atli, A.; Alnot, M.; Ehrhardt, J. J.; Bertolini, J. C.; Abon, M. *Surf. Sci.* **1992**, *270*, 365.
(127) Kitchin, J. R.; Nørskov, J. K.; Barteau, M. A.; Chen, J. G. *J. Chem. Phys.* **2004**, *120*, 10240.
(128) Beutl, M.; Lesnik, J.; Rendulic, K. D.; Hirschl, R.; Eichler, A.; Kresse, G.; Hafner, J. *Chem. Phys. Lett.* **2001**, *342*, 473.
(129) Schennach, R.; Krenn, G.; Klötzer, B.; Rendulic, K. D. *Surf. Sci.* **2003**, *540*, 237.
(130) Greeley, J.; Mavrikakis, M. *Nat. Mater.* **2004**, *3*, 810.
(131) Amandusson, H.; Ekedahl, L. G.; Dannetun, H. *J. Membr. Sci.* **2001**, *193*, 35.
(132) Alfonso, D. R.; Cugini, A. V.; Sholl, D. S. *Surf. Sci.* **2003**, *546*, 12.
(133) In *Hydrogen in Metals II*; Alefeld, G., Völkl, J., Eds.; Springer-Verlag: Berlin, 1978; Vol. 29.
(134) Bowman, R. C., Jr.; Fultz, B. *MRS Bull.* **2002**, *27*, 688.
(135) Johnson, A. D.; Daley, S. P.; Utz, A. L.; Ceyer, S. T. *Science* **1992**, *257*, 223.
(136) Hammer, B.; Hansen, L. B.; Nørskov, J. K. *Phys. Rev. B: Condens. Matter Mater. Phys.* **1999**, *59*, 7413.
(137) Neugebauer, J.; Scheffler, M. *Phys. Rev. B: Condens. Matter Mater. Phys.* **1992**, *46*, 16067.
(138) Vanderbilt, D. *Phys. Rev. B: Condens. Matter Mater. Phys.* **1990**, *41*, 7892.
(139) Perdew, J. P.; Chevary, J. A.; Vosko, S. H.; Jackson, K. A.; Pederson, M. R.; Singh, D. J.; Fiolhais, C. *Phys. Rev. B: Condens. Matter Mater. Phys.* **1992**, *46*, 6671.
(140) White, J. A.; Bird, D. M. *Phys. Rev. B: Condens. Matter Mater. Phys.* **1994**, *50*, 4954.
(141) Kresse, G.; Furthmuller, J. *Comput. Mater. Sci.* **1996**, *6*, 15.
(142) Lide, D. R. *CRC Handbook of Chemistry and Physics*, 76th ed.; CRC Press: New York, 1996.
(143) Ruban, A. V.; Skriver, H. L.; Nørskov, J. K. *Phys. Rev. B: Condens. Matter Mater. Phys.* **1999**, *59*, 15990.
(144) Mavrikakis, M.; Rempel, J.; Greeley, J.; Hansen, L. B.; Nørskov, J. K. *J. Chem. Phys.* **2002**, *117*, 6737.
(145) Krekelberg, W. P.; Greeley, J.; Mavrikakis, M. *J. Phys. Chem. B* **2004**, *108*, 987.

(146) Arnold, M.; Sologub, S.; Frie, W.; Hammer, L.; Heinz, K. *J. Phys.: Condens. Matter* **1997**, *9*, 6481.
(147) Jachimowski, T. A.; Meng, B.; Johnson, D. F.; Weinberg, W. H. *J. Vac. Sci. Technol., A* **1995**, *13*, 1564.
(148) Conrad, H.; Ertl, G.; Latta, E. E. *Surf. Sci.* **1974**, *41*, 435.
(149) Tamm, P. W.; Schmidt, L. D. *J. Chem. Phys.* **1971**, *54*, 4775.
(150) Yates, J. T.; Thiel, P. A.; Weinberg, W. H. *Surf. Sci.* **1979**, *84*, 427.
(151) Mahnig, M.; Schmidt, L. D. *Z. Phys. Chem.* **1972**, *80*, 71.
(152) Bozso, F.; Ertl, G.; Grunze, M.; Weiss, M. *Appl. Surf. Sci.* **1977**, *1*, 103.
(153) Bridge, M. E.; Comrie, C. M.; Lambert, R. M. *J. Catal.* **1979**, *58*, 28.
(154) Frühberger, B.; Eng, J.; Chen, J. G. *Catal. Lett.* **1997**, *45*, 85.
(155) Šljivančanin, Ž.; Hammer, B. *Phys. Rev. B: Condens. Matter Mater. Phys.* **2002**, *65*, 85 414.
(156) Sakong, S.; Gross, A. *Surf. Sci.* **2003**, *525*, 107.
(157) Hammer, B.; Nørskov, J. K. *Nature* **1995**, *376*, 238.
(158) Greeley, J.; Mavrikakis, M. *Surf. Sci.* **2003**, *540*, 215.
(159) Greeley, J.; Krekelberg, W. P.; Mavrikakis, M. *Angew. Chem., Int. Ed.* **2004**, *43*, 4296.